Quantum algorithm for simulating an experiment: Light interference from single ions and their mirror images

Luc Bouten,[1,*] Gé Vissers,[1,†] and Ferdinand Schmidt-Kaler[2]
[1]*Q1t BV, Lindenlaan 15, 6584 AC, Molenhoek, The Netherlands*
[2]*QUANTUM, Institut für Physik, Johannes Gutenberg-Universität Mainz, Staudingerweg 7, 55128 Mainz, Germany*

(Received 14 May 2019; published 20 August 2019)

We widen the range of applications for quantum computing by introducing digital quantum simulation methods for coherent light-matter interactions: We simulate an experiment where the emitted light from a single ion was interfering with its mirror image [Eschner *et al.*, Nature (London) **413**, 495 (2001)]. Using the quantum simulation software Q1TSIM, we accurately reproduce the interference pattern which had been observed experimentally and also show the effect of the mirror position on the spontaneous-emission rate of the ion. In order to minimize the number of required qubits, we implement a qubit-reinitialization technique. We show that a digital quantum simulation of complex experiments in atomic and quantum physics is feasible with no more than six qubits, a setting which is well within reach for advanced quantum computing platforms.

DOI: 10.1103/PhysRevA.100.022323

I. INTRODUCTION

Typical applications of quantum simulation include open questions in solid-state physics [1–3]. More recently, using trapped-ion setups, high-energy physics problems have been addressed in experimental quantum simulation [4–6] and, in hybrid classical-quantum simulations, solutions to molecular chemistry calculations have been demonstrated [7,8]. Yet another set of applications has investigated energy transport in the quantum regime, with implications for our understanding of biological systems [9–11]. Experimental realizations of open quantum systems require the ability to implement both coherent many-body dynamics and dissipative processes [12,13]. Quantum simulation has been proposed even for mimicking nonphysical systems [14]. Using a superconducting circuit quantum computer, problems in the financial sector have been addressed, e.g., for an analysis of market stability or for pricing financial derivatives [15,16].

Here, we widen the spectrum of applications for digital quantum simulation further and propose to digitally simulate an experimental outcome. Specifically, we are able to accurately reproduce on a simulator of a quantum computer the outcome of a trapped-single-ion experiment, where an interference pattern has been observed experimentally [17]. We show in our simulations—similar to the experiment—the strong influence of the mirror position on the spontaneous-emission rate of the ion. Implementing an experimental setting which includes the coherent emission and absorption of a quantum light field, the optical excitation of two-level systems, the interference of light, and backaction on the atomic electronic levels, we provide a wide and universal set of tools for digital simulation which may therefore be applied to predict results in many other atomic, ionic, molecular, and optical experiments.

For simulating light-matter interactions in a digital quantum simulator, we divide the electromagnetic field into spatial slices, each containing either zero or one photon, or any coherent superposition of these states. In this way, the field is modeled by a tensor network of qubits. At the points where the electromagnetic field interacts with matter, e.g., a single atom, ion, or a collection of atomic emitters, we introduce a unitary interaction matrix that couples the field slice at that position with the matter system. This unitary interaction represents one time step of the simulation. As the electromagnetic field is propagating with the speed of light, qubits in the tensor network move to the next field slice in every new time step of the computation. The tensor network might contain loops, which means we can also model fully coherent feedback, e.g., when back reflecting the emitted light by semicavities.

The paper is organized as follows: After sketching the experimental setup to be implemented by quantum simulation, we describe the model and its approximations. We continue with a detailed discussion of the simulation calculation method and exemplify the accuracy of results from the fitting parameters to the simulated interference pattern, in comparison with the experimental findings.

II. THE MODEL

As a case example of our open-system quantum simulation, we model an experiment [17] in which a single ion is held in a Paul trap in front of a mirror. When laser exciting the ion, resonance fluorescence is emitted and two light paths towards a detector are established: light that returns to the ion via the mirror before arriving at the detector, and light directly being detected. If the optical path lengths of these two light paths differ by a noninteger multiple of the transition wavelength, there will be destructive interference. By mounting the mirror on a piezoelectric stage and varying the distance to the mirror, an interference pattern as a function of the distance was observed.

*www.q1t.nl
†Corresponding author: ge@q1t.nl

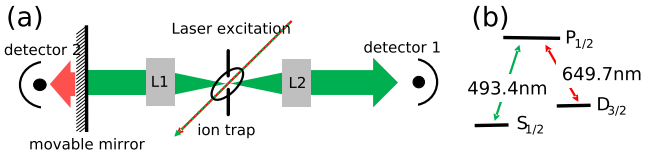

FIG. 1. Setup: (a) A single barium$^+$ ion is trapped in a Paul trap. The Ba^+ ion is driven on its $S_{1/2} \leftrightarrow P_{1/2}$ transition of 493 nm (green). The Ba^+ ion emits fluorescence photons directly to a photodetector, via the focusing lens L2, and towards a mirror reflecting 493 nm radiation. The light that travels towards the mirror is turned into a collimated beam via the collimating lens L1. In this way, two light paths of different optical lengths towards the photodetector are created. The mirror position can be actuated by a piezoelectric stage and, as such, we can control the difference in optical path length between the two light paths, revealing an interference pattern at the photodetector [17]. The $P_{1/2} \leftrightarrow D_{3/2}$ transition near 650 nm is detected in detector 2, and allows for revealing the population in $P_{1/2}$. (b) Scheme of relevant levels and transitions.

In the experiment, a single Ba^+ ion is continuously laser excited and laser cooled on its $S_{1/2} \leftrightarrow P_{1/2}$ and $P_{1/2} \leftrightarrow D_{3/2}$ resonance lines of 493 and 650 nm, respectively; see Fig. 1. For the quantum simulation, we ignore the $D_{3/2}$ state and model the Ba^+ ion as a two-level system at a fixed position in space. The excitation of the transition $S_{1/2}$ to $P_{1/2}$ induces Rabi oscillations as well as the emission of fluorescence photons near 493 nm, which are subsequently collected by two lenses. One lens collimates the light that is directed towards the mirror, such that light can reinteract after a time delay and the second lens focuses the outgoing light in the direction of the photodetector 1 [17]; see Fig. 1(a).

The coordinates are fixed such that the Ba^+ ion is located at the origin and we place the reflection at a position $-d$. This leads to a natural timescale: we define T as the time it takes for a photon to make a round trip from the Ba^+ ion to the mirror and back, i.e., $T := 2d/c$, where c stands for the speed of light. We divide the time interval $[0, T]$ in $N \in \mathbb{N}$ equal time slices and we define a discretization parameter λ by

$$\lambda := \sqrt{\frac{T}{N}}, \tag{1}$$

such that every time slice represents λ^2 seconds.

We divide the field, interacting with the single ion, into three channels: (C1) photons traveling from the ion to the mirror, (C2) photons returning from the mirror to the ion, and (C3) laser light from the side exciting the ion. All three channels are represented by a doubly infinite string of qubits; see Fig. 2. The free time evolution Θ of the electromagnetic field C1 and C3 corresponds to left shift, i.e., in one time step, all elements in the tensor network shift left by one position. For C2, a free time evolution time step is imaged as a shift to the right; see Fig. 2.

We now introduce an interaction $R: \mathbb{C}^2 \otimes \mathbb{C}^2 \otimes \mathbb{C}^2 \to \mathbb{C}^2 \otimes \mathbb{C}^2 \otimes \mathbb{C}^2$ between the Ba^+ ion and the field slices at the origin of the channels 1 and 2 (last two copies of $\mathbb{C}^2$ in the tensor product),

$$R := e^{\sqrt{\kappa}\lambda(\sigma_- \otimes I \otimes \sigma_+ - \sigma_+ \otimes I \otimes \sigma_-)} e^{\sqrt{\kappa}\lambda(\sigma_- \otimes \sigma_+ \otimes I - \sigma_+ \otimes \sigma_- \otimes I)}. \tag{2}$$

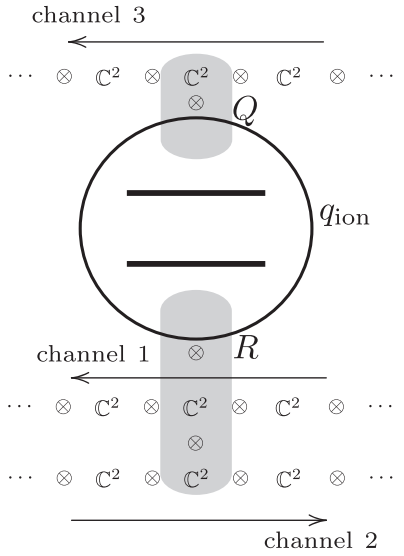

FIG. 2. Model: The ion is represented by the qubit at the center, labeled q_{ion}. Channel 1 represents the photons that are moving left towards the mirror. Channel 2 represents the photons that are moving to the right towards the photodetector. Channel 3 is the side channel for laser driving the ion. Note that in the tensor network, the side channel (channel 3) has also been represented horizontally such that the network can be better visualized. Interactions Q between laser and the ion, and R between the ion and the two-photon field channels, occur at the origin.

Here, κ is the strength of the coupling between the Ba^+ ion and the two field channels. Without loss of generality, we assume identical coupling strength for C1 and C2, corresponding to an identical focusing by lenses L1 and L2. Operators σ_+ and σ_- denote the standard raising and lowering operators on a two-level system.

We introduce the interaction $Q: \mathbb{C}^2 \otimes \mathbb{C}^2 \to \mathbb{C}^2 \otimes \mathbb{C}^2$ between the Ba^+ ion and the laser field slice at the origin of the third channel,

$$Q := e^{\sqrt{\kappa_s}\lambda(\sigma_- \otimes \sigma_+ - \sigma_+ \otimes \sigma_-)}, \tag{3}$$

where κ_s is the coupling strength between the Ba^+ ion and the side channel C3. Furthermore, the Ba^+ ion undergoes its own internal time evolution given by

$$L := e^{-i\omega\sigma_+\sigma_-\lambda^2}. \tag{4}$$

We initialize all field slices in C1 and C2 in the vacuum state before interaction with the ion. The side channel C3, however, is initialized in a coherent state representing the resonantly driving laser. A complex number $\alpha = |\alpha| e^{-i\omega l\lambda^2}$ represents its amplitude and phase, where l represents the time step. We now introduce the discrete Weyl (or displacement) operator acting on the qubit at the origin of C3,

$$M := e^{\lambda\alpha\sigma_+ - \lambda\bar{\alpha}\sigma_-}. \tag{5}$$

Acting with the operator M on the vacuum vector of the slice of C3 at the origin, we drive this slice in a coherent state that represents the resonant driving laser. In this way, Rabi oscillations are induced in the ion with frequency $\Omega = |\alpha|\sqrt{\kappa_s}$.

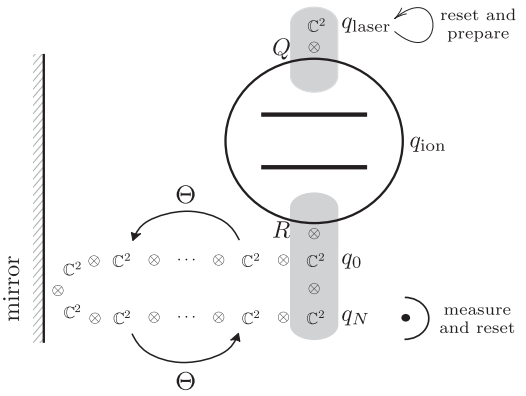

FIG. 3. Closed-loop interaction model: Initially, the laser qubit q_{laser} interacts with the Ba^+ ion qubit q_{ion} through interaction Q. Next, the ion interacts with the first and last field qubits q_0 and q_N through interaction R. Afterwards, q_{laser} is reset, the outgoing field qubit q_N is measured and reset, and the field qubits are shifted.

Combining contributions from Eqs. (2)–(5), we construct a time evolution which is given by an evolution $U_l := (\Theta LRQM)^l$. Repeated interactions as described by this evolution have been studied in the literature [18–26] and it can be shown that such a repeated interaction converges to a Hudson-Parthasarathy quantum stochastic differential equation (QSDE) [27] in the limit where the discretization parameter λ goes to 0. In fact [20–22,25], every QSDE can be approximated (using the same field discretization) by repeated interaction of unitaries that can be implemented as gates on a quantum computer. As such, the methods used in this paper are much more widely applicable than just the experiment studied in this paper, since QSDEs are ubiquitous in quantum optics. Examples of systems described by a QSDE can be found in electron shelving [28], Stark splitting in fluorescent spectra [29], Faraday rotation experiments [30], and cavity QED [31,32].

QSDEs constitute the starting point for the quantum stochastic input-output formalism introduced by Gardiner and Collett [33]. Consequently, our quantum simulation may be interpreted as a discretization of input-output open quantum systems, optionally creating finite loops by connecting some of the inputs to some of the outputs. In this specific case, this is the back reflection of photons in C1 by the mirror to interact again with the ion as C2.

At the mirror, the field slices of C1 are transferred to C2. In this way, a loop of $N+1$ field qubits $q_0 \dots q_N$ is created; see Fig. 3. In the experiment [17], the mirror is placed at a distance of about 0.25 m; however, modeling such a long time delay would require a prohibitively large number of qubits in C1 and C2. Instead, we limit the distance d to the wavelength of the atomic transition and capture two full cycles of the interference pattern. Note that by varying d for given N, we also vary the time step λ according to Eq. (1).

As soon as the last qubit q_N in C2 has interacted with the ion, we project it in the σ_z basis. If the measurement result is $+1$, we rotate the qubit back to $|0\rangle$. Then, the qubit is shifted to C1 at the origin. In this way, we reinitialize the qubit and can reuse it in the quantum computation, keeping the total required number of qubits minimal. Employing a similar procedure for C3, we can simulate the entire channel with a single qubit; see Fig. 3.

In the following, we assume a six-qubit quantum computer, such that one qubit represents the ion, one represents the laser, and the other four are used to model the electromagnetic field.

III. QUANTUM CIRCUIT

To implement the interaction described by the evolution U_l, all contributions are mapped to elementary single- and two-qubit gate operations. Leaving the interaction R between the ion and the two-photon field slices unspecified for the moment, the circuit for time step l is given by

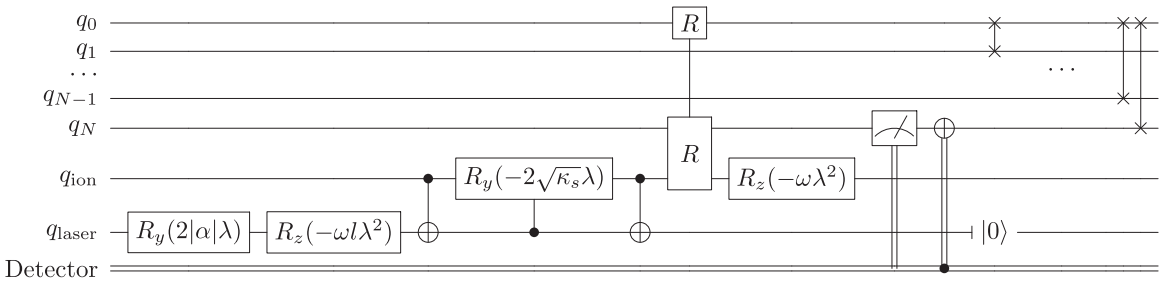

(6)

Here the first two rotation gates represent the initialization of the laser. Note that the $R_z(-\omega l\lambda^2)$ rotation setting the phase of the laser qubit is different for each time step. The subsequent three controlled gates simulate the interaction of the driving laser with the ion. Next follows the interaction of the ion with the photon field slices, and the internal evolution of the atom. Finally, the outgoing field slice is measured and reset, the laser qubit is reset, and the field slices are shifted by a series of SWAP gates.

Note that the shifting of field qubits only results in a relabeling of the qubits, and is only included here so that the interaction looks the same for each time step. In a practical simulation on a real quantum computer, one could omit the SWAP gates and simply interact with and measure different field qubits in each time step.

The interaction R between the ion and the photon field, given by Eq. (2), can be decomposed into elementary quantum gates as follows:

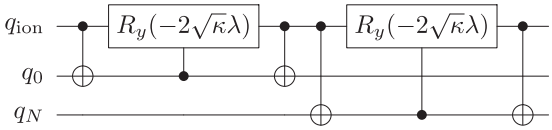

(7)

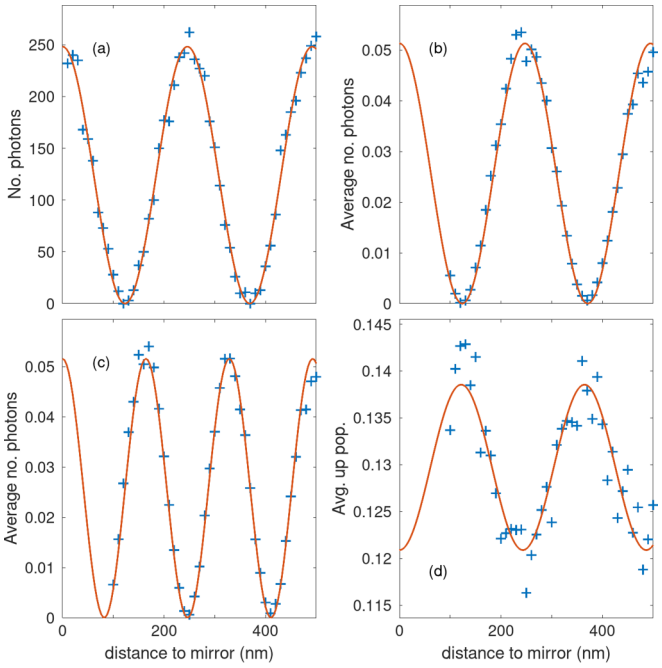

FIG. 4. Simulation results: (a) Calculated number of emitted photons after 25 ps, single run, with $\omega = 1.0f$; (b) after 20 fs, averaged over 1 00 000 runs, with $\omega = 1.0f$; (c) after 20 fs, averaged over 1 00 000 runs, with $\omega = 1.5f$; (d) population of the upper state after 20 fs, time averaged and averaged over 1 00 000 runs. We use the same parameters as in (b). Here, f is the transition frequency of the Ba^+ ion (493 nm). The other parameters used in the calculation are $1 \leqslant N \leqslant 3$, $\Omega = 0.01f$, $\kappa = 6 \times 10^{12}$, and $\kappa_s = 3 \times 10^{13}$, for all panels. Calculated results from the simulations are indicated by crosshair markers; solid lines show the fit. The fitted wavelengths are (a) 246.0, (b) 247.4, (c) 164.3, and (d) 243.2 nm.

IV. RESULTS AND DISCUSSION

We have implemented the quantum circuit from Eq. (6) on a quantum computer simulator developed by Q1t BV, called Q1TSIM [34].

Two types of calculations have been performed. A direct simulation of the experiment was done by running over a long time period (25 ps), but using only a single run. In the second type of calculation, we have chosen parameters more conducive to running on a real quantum computer, simulating only 20 fs and distances $d \geqslant 100$ nm, but averaging the results over multiple runs.

We set the transition frequency in the ion to the experimental value of $f = 2\pi c/493$ nm. To show that our approach may be experimentally feasible to implement on current-technology quantum computers, we restricted the calculations to using up to four qubits for representing the photon field. More specifically, two field qubits were used for mirror distances $d < 170$ nm, three field qubits for $170 \leqslant d < 260$ nm, and four for $d \geqslant 260$ nm.

The results for the simulations are shown in Figs. 4(a) and 4(b). Both simulations clearly show the interference pattern that has been previously observed in the experiment [17]. Fitting the oscillation frequency of the interference pattern, we find 246.0 and 247.4 nm, respectively, both close to the expected value of $493/2$ nm $= 246.5$ nm.

To prove that the observed pattern is indeed caused by interference, we have performed calculations with the value of the internal transition frequency raised to $\omega = 1.5f$. The results are shown in Fig. 4(c). As expected, the fit for the wavelength of the interference pattern of 164.3 nm is shorter by the factor 1.5.

More interestingly, the interaction with the back-reflected photon channel does not only result in an interference pattern, but its backaction affects the emission rate of the ion to be either enhanced or reduced, depending on the ion-to-mirror distance. This results in a modulation of the $P_{1/2}$ state occupation probability, which has been revealed from the observation of photons near 650 nm on the $P_{1/2}$-to-$D_{3/2}$ transition [17]. The mirror coating in the experimental realization was chosen highly transmitting near 650 nm such that the detector 2 allows one to detect such photons; see Fig. 1. To illustrate that our simulation captures this behavior, the calculated population of the upper state of the ion is evaluated, as a function of the distance, and averaged over time and 1 00 000 runs; see Fig. 4(d). It is easily seen that the $P_{1/2}$ lifetime of the ion perfectly anticorrelates with the emitted photon count rate at 493 nm.

Using the full circuit defined by Eqs. (6) and (7), a single time step in the simulation requires three single-qubit operations, nine two-qubit operations, and two measurement operations, where controlled rotations are each counted as one two-qubit operation and the SWAP gates are omitted. The number of time steps needed depends on the number of qubits used to represent the field, and the distance to the mirror. For the results in Fig. 4(b), between 18 and 35 steps have been taken for each data point to simulate up to 25 fs. Implementing these circuits would require up to 105 single-qubit and 315 two-qubit operations.

V. CONCLUSION AND OUTLOOK

We have been able to reproduce the interference pattern which had been observed in experiment [17] using the Q1TSIM simulator of a quantum computer. Furthermore, we have shown that the presence of the mirror modifies the emission by, and thus the lifetime of, an excited state of the Ba^+ ion. Our results demonstrate simulation of a quantum model including a coherent feedback loop on a quantum computer. Using the methods we presented in this paper, it will be possible to model many more problems originating from quantum optics and, more specifically, cavity QED, on a future quantum computer.

Furthermore, we demonstrated that qubit reinitialization within a computation run allows for reducing the number of required qubits, thus facilitating a simulation of the experiment [17] with $\leqslant$10 qubits. Circuits we have been simulating on the Q1TSIM simulator are ready to be implemented in the laboratory on state-of-the-art platforms.

[1] A. Trabesinger, Nat. Phys. **8**, 263 (2012).

[2] T. Schaetz, C. R. Monroe, and T. Esslinger, New J. Phys. **15**, 085009 (2013).

[3] I. M. Georgescu, S. Ashhab, and F. Nori, Rev. Mod. Phys. **86**, 153 (2014).

[4] R. Gerritsma, B. P. Lanyon, G. Kirchmair, F. Zähringer, C. Hempel, J. Casanova, J. J. García-Ripoll, E. Solano, R. Blatt, and C. F. Roos, Phys. Rev. Lett. **106**, 060503 (2011).

[5] E. Martinez, C. Muschik, P. Schindler, D. Nigg, A. Erhard, M. Heyl, P. Hauke, M. Dalmonte, T. Monz, P. Zoller *et al.*, Nature (London) **534**, 516 (2016).

[6] C. Muschik, M. Heyl, E. Martinez, T. Monz, P. Schindler, B. Vogell, M. Dalmonte, P. Hauke, R. Blatt, and P. Zoller, New J. Phys. **19**, 103020 (2017).

[7] C. Hempel, C. Maier, J. Romero, J. McClean, T. Monz, H. Shen, P. Jurcevic, B. P. Lanyon, P. Love, R. Babbush *et al.*, Phys. Rev. X **8**, 031022 (2018).

[8] Y. Nam, J.-S. Chen, N. C. Pisenti, K. Wright, C. Delaney, D. Maslov, K. R. Brown, S. Allen, J. M. Amini, J. Apisdorf *et al.*, arXiv:1902.10171.

[9] D. J. Gorman, B. Hemmerling, E. Megidish, S. A. Moeller, P. Schindler, M. Sarovar, and H. Haeffner, Phys. Rev. X **8**, 011038 (2018).

[10] S. Debnath, N. M. Linke, S.-T. Wang, C. Figgatt, K. A. Landsman, L.-M. Duan, and C. Monroe, Phys. Rev. Lett. **120**, 073001 (2018).

[11] C. Maier, T. Brydges, P. Jurcevic, N. Trautmann, C. Hempel, B. P. Lanyon, P. Hauke, R. Blatt, and C. F. Roos, Phys. Rev. Lett. **122**, 050501 (2019).

[12] M. Müller, K. Hammerer, Y. L. Zhou, C. F. Roos, and P. Zoller, New J. Phys. **13**, 085007 (2011).

[13] P. Schindler, M. Müller, D. Nigg, J. Barreiro, E. Martinez, M. Hennrich, T. Monz, S. Diehl, P. Zoller, and R. Blatt, Nat. Phys. **9**, 361 (2013).

[14] T. E. Lee, U. Alvarez-Rodriguez, X.-H. Cheng, L. Lamata, and E. Solano, Phys. Rev. A **92**, 032129 (2015).

[15] R. Orús, S. Mugel, and E. Lizaso, Phys. Rev. A **99**, 060301 (2019).

[16] A. Martin, B. Candelas, Á. Rodríguez-Rozas, J. D. Martín-Guerrero, X. Chen, L. Lamata, R. Orús, E. Solano, and M. Sanz, arXiv:1904.05803.

[17] J. Eschner, C. Raab, F. Schmidt-Kaler, and R. Blatt, Nature (London) **413**, 495 (2001).

[18] B. Kümmerer, J. Funct. Anal. **63**, 139 (1985).

[19] K. R. Parthasarathy, J. Appl. Probab. **25A**, 151 (1988).

[20] J. M. Lindsay and K. R. Parthasarathy, Sankhya: Indian J. Stat., Series A (1961-2002) **50**, 151 (1988).

[21] S. Attal and Y. Pautrat, Ann. Henri Poincaré **7**, 59 (2006).

[22] L. M. Bouten and R. van Handel, J. Math. Phys. **49**, 102109 (2008).

[23] L. M. Bouten, R. van Handel, and M. James, SIAM Rev. **51**, 239 (2009).

[24] A. Belton, M. Gnacik, and J. Lindsay, Ann. Henri Poincaré **19**, 1711 (2018).

[25] G. Vissers and L. Bouten, Quantum Inf. Proc. **18**, 152 (2019).

[26] J. Gough and M. James, IEEE Trans. Autom. Control **54**, 2530 (2009).

[27] R. L. Hudson and K. R. Parthasarathy, Commun. Math. Phys. **93**, 301 (1984).

[28] A. Barchielli, J. Phys. A **20**, 6341 (1987).

[29] P. Robinson and H. Maassen, Rep. Math. Phys. **30**, 185 (1991).

[30] L. Bouten, J. Stockton, G. Sarma, and H. Mabuchi, Phys. Rev. A **75**, 052111 (2007).

[31] L. Bouten, R. van Handel, and A. Silberfarb, J. Funct. Anal. **254**, 3123 (2008).

[32] J. Kerckhoff, L. Bouten, A. Silberfarb, and H. Mabuchi, Phys. Rev. A **79**, 024305 (2009).

[33] C. W. Gardiner and M. J. Collett, Phys. Rev. A **31**, 3761 (1985).

[34] Q1t BV, `q1tsim` quantum computer simulator, https://crates.io/crates/q1tsim, https://github.com/Q1tBV/q1tsim (2019), version 0.3 (unpublished).